VOL. 13, NO. 23, DECEMBER 2018 ISSN 1819-6608
ARPN Journal of Engineering and Applied Sciences

www.arpnjournals.com

BATTERY ENERGY STORAGE FOR VARIABLE SPEED PHOTOVOLTAIC WATER PUMPING SYSTEM

Ahmed Moubarak, Gaber El-Saady and El-Noby A. Ibrahim
Department of Electrical Engineering, Faculty of Engineering, Assiut University, Egypt
E-Mail: ahmedalaa.ck7@gmail.com

ABSTRACT

The photovoltaic (PV) solar electricity is no longer doubtful in its effectiveness in the process of rural communities' livelihood transformation with solar water pumping system being regarded as the most important PV application. To overcome the intermittent and uncertain nature of solar power output, the highly fluctuating load demands and to supply loads at night time, a battery storage system is optimally sized, designed and implemented. The bi-directional Buck-Boost converter use and control are essential for energy management between the batteries and the pumping system. Domestic loads power calculation is also demonstrated and varied. Additionally, various inverter control schemes are examined and employed depending on the nature of the load connected. Finally, simulation results using Matlab/Simulink are presented for two cases: when the battery system is connected with the PV array to feed the pump motor to achieve the required varying hydraulic performance (flow rate and pumping head) under different weather conditions, and when the battery system feeds the loads while the PV array is disconnected at night.

Keywords: battery control topologies, bi-directional DC-DC converter, lithium-ion battery, photovoltaic pumping.

1. INTRODUCTION

Photovoltaic (PV) energy is now becoming one of the fastest growing renewable energy technologies as there have been several major advancements in solar cells design, and large scale manufacturing techniques, as well as new developments in system component technology. It is estimated that the PV electricity will contribute with 7% of the world electricity needs by the year 2030, and this will increase to reach 25% by the year 2050 [1]. The most common PV application is solar water pumping [2, 3]. The energy extracted from the PV modules depend on weather conditions. These modules have an optimum operating point, called the maximum power point, which depends on the intensity of illumination. In order to extract maximum power from these modules, they are connected to a DC–DC converter controlled by maximum power point tracking (MPPT) techniques [4, 5]. The most frequently encountered machine used in solar water pumping systems is the three phase induction motor. Its popularity is due to its capability of producing high power, simple design, and it's easy to maintain [6]. The DC/AC voltage source inverter (VSI) is employed to feed the motor driving the centrifugal pump [7]. The Affinity laws are mathematical relationships that allow for the estimation of changes in pump performance as a result of a change in one of the basic pump parameters. This is done by changing the pump speed, and consequently, the pump flow rate, head, and power will be varied [8].

The method proposed by [3] is a new one where the water pump is able to accommodate for the desired hydraulic requirements (pumping flow rate and head) when the pump motor is fed only from the PV array without any connection to other power sources or energy storage systems. Although this method is fairly effective, it has some limitations, namely it can't achieve high values of both flow rate and pumping head at the same time due to the fixed power source, and it doesn't take full advantage of the Affinity laws capability which relates to energy conservation and efficiency. A battery storage system is designed to mitigate these issues. The batteries will aid the pump in achieving its desired hydraulic requirements fully and without limitations. This, in turn, will help in reaping the full benefits of the Affinity laws where the required motor power will change with changing the pumping head or the flow rate. Furthermore, the bi-directional power transfer capability of the battery storage system and the Affinity laws will provide protection for the pump motor where the motor power will decrease when the pump motor speed decreases and vice versa. In addition, batteries can be used to store the output energy during times of surplus power generation and distributed at the time of peak energy demand or loss of supply conditions. The entire system of energy management involves equilibrium in the supply and end users energy demand service sustainability. At the point of generation, energy produced may need to be stored especially at night when there is no sunlight where the PV modules won't be able to generate any power and the battery units will be the only source of power available to feed domestic loads.

2. THE PROPOSED SYSTEM

The battery storage system for the PV water pumping system is shown in Figure-1.

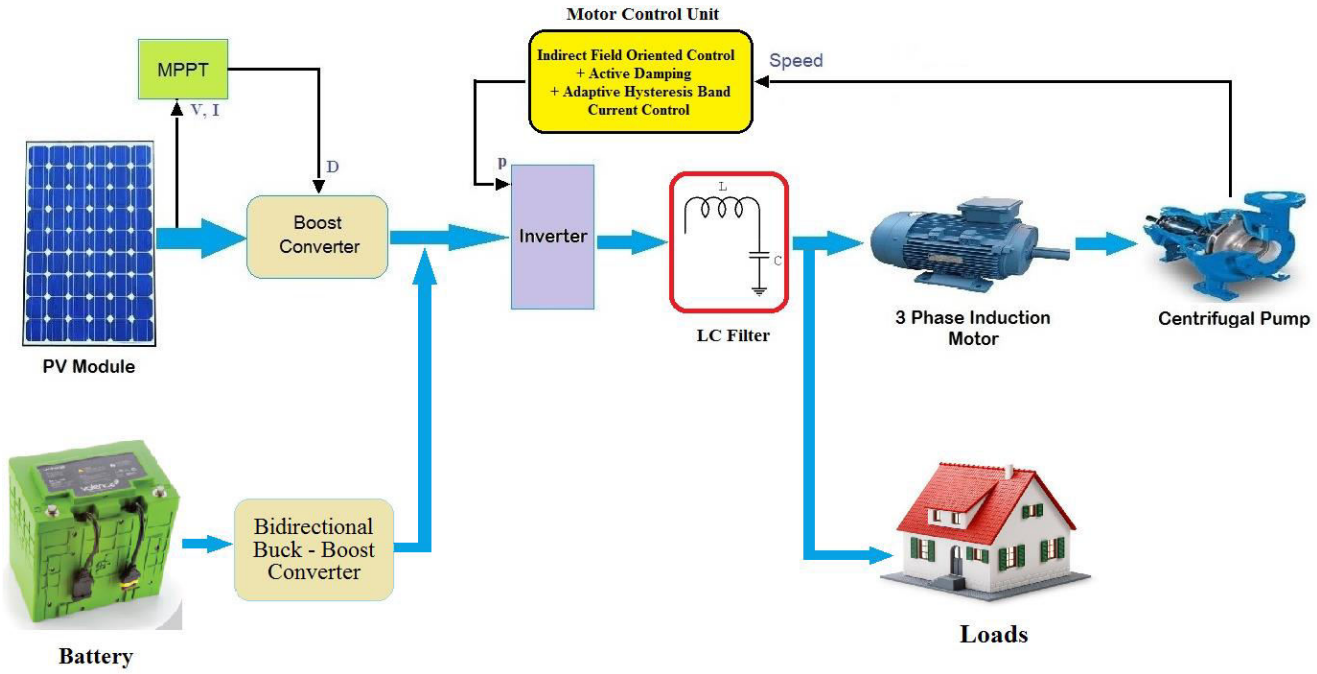

Figure-1. Battery storage system for the PV water pumping system.

The PV data, Boost DC-DC converter calculation and values, MPPT topology, VSI control technique and the motor-pump set (three phase induction motor driving a centrifugal pump) parameters are all fully demonstrated in [3]. Additionally, a thorough explanation of the inclusion and function of the LC filter which is connected between the VSI and the loads to mitigate the noise and harmonics as well as the active damping technique and the adaptive hysteresis band current control method are given in [9].

Furthermore, the batteries are used as a backup energy storage system to make the power available through the night or bad weather conditions. A bi-directional Buck-Boost converter is used with the battery system to help in the charging and discharging processes. Finally, domestic (AC) loads are present in this system.

3. BATTERY MODELING

Battery models are employed in battery characterization, state of charge (SOC), algorithm development, system-level optimization, and real-time simulation for battery management system design. The battery type chosen in this study is of type Lithium-ion (Li-ion). Lithium based batteries with their technical characteristics have the potential to revolutionize the PV industry and renewable energies in general. Advantages of Li-ion batteries compared to other battery types relate to their high-energy efficiency, high power density, no memory effects, high reliability and a relatively long cycle life.

A detailed mathematical battery model normally includes several sub-models. The most vital sub-model for electrical system study is the voltage-current model, which describes how the terminal voltage of a battery changes with the current. The best known approach is to use pre-established mathematical relationships to model fundamental relationships between terminal voltage, current and battery state of charge (SOC). The model of Tremblay [10], which is based on Shepherd's equation [11], is an example. It has the advantage of only requiring three points on the constant current discharge curve typically included in the battery's data sheets to extract the model's parameters. The equivalent circuit of a generic dynamic Li-ion battery model as developed by [10] is shown in Figure-2.

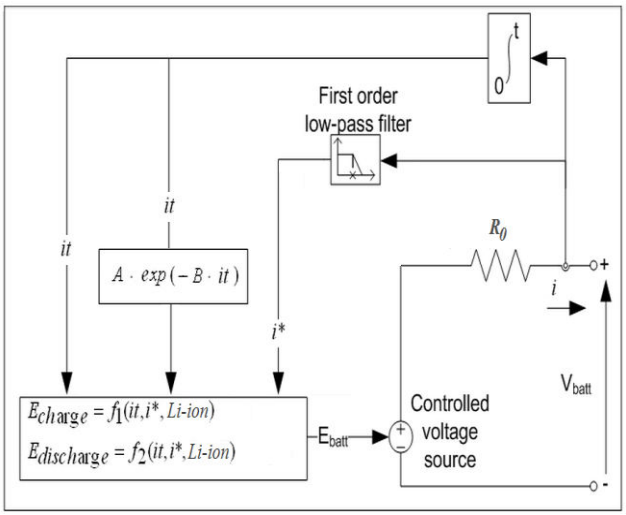

Figure-2. Equivalent circuit of Li-ion battery.

4. BI-DIRECTIONAL DC-DC CONVERTER

For a two-way energy flow from and to the battery system, a bi-directional (Buck-Boost) DC-DC converter is used as presented in this section.

4.1 Bi-directional converter topology

Battery storage devices require bi-directional DC-DC interface to control their charging and discharging processes. The converter used in this study is a half-bridge IGBT topology, or two-quadrant class D chopper, operating in continuous conduction mode (CCM) as shown in Figure-3. The half-bridge converter has the advantage that the number of components that are subjected to high currents and/or voltages is reduced in comparison to the other configurations [12]. The number of power components increases losses in the converter as well as producing costs. The half-bridge is also favorable since the stresses over the active components are reduced.

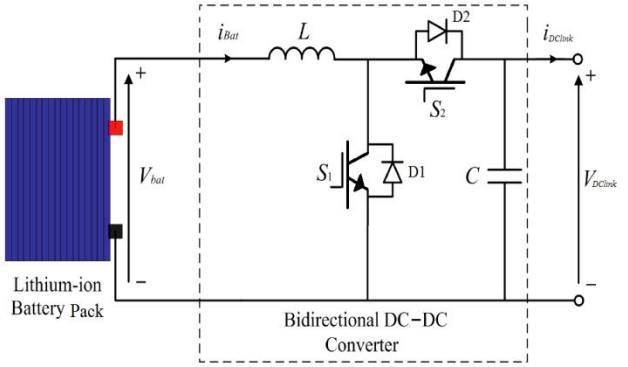

Figure-3. Bi-directional half bridge DC-DC converter.

The topology operates in Boost-mode for battery discharging operation, or in Buck-mode in cases of battery charging. The DC-link current (i_{DClink}) is either positive or negative and the voltage across the bus is always positive.

In Boost-mode, S1 and D2 are active and the current flows to the DC-link. In Buck-mode, S2 and D1 are active and the power flow is reversed.

4.2 Calculation of the power inductor value

The power inductance estimation is done considering the bi-directional converter operating in both modes, Buck and Boost, under limited conditions, for CCM operation and for a maximum current ripple, ΔI_L of 10%.

When the bi-directional converter operates in Buck-mode, the worst condition occurs when V_{DClink} is at its maximum (V_{DClink_max}) and the battery voltage is at its minimum value (V_{batt_min}). Normal operation occurs when the battery voltage is at its maximum value (V_{batt_max}) and V_{DClink} is at its nominal value. When the bi-directional converter operates in Boost-mode, the worst condition occurs when V_{DClink} is at its nominal value, and the battery voltage is at its minimum value. Normal operation is the same as the Buck-mode. Cases where V_{DClink} is at its minimum value only occur when the supply sources are not capable of responding to the load power demand, or during load variations. In this last case, the converter voltage controller will induce a higher current reference in order to restore the nominal DC-link voltage value. These variations can be neglected for the inductor design due to their occasional nature. The largest obtained inductance value will serve as reference for the power inductor prototype [12].

- For Buck-mode:

$$L = \frac{V_{batt}\,(1-D)}{\Delta I_L f_s} \quad (1)$$

Where D varies between D_{min} and D_{max}, but D_{min} will be used to obtain a higher inductance value.

And:

$$D_{min} = \frac{V_{batt\_min}}{V_{DClink\_max}} \quad (2)$$

- For Boost-mode:

In this case, L_{min} and L_{max} should be considered.

$$L_{min} = \frac{V_{batt\_min} D_{max}}{\Delta I_L f_s} \quad (3)$$

$$L_{max} = \frac{V_{batt\_max} D_{min}}{\Delta I_L f_s} \quad (4)$$

And:

$$D_{min} = 1 - \frac{V_{batt\_max}}{V_{DClink}} \quad (5)$$

$$D_{max} = 1 - \frac{V_{batt\_min}}{V_{DClink}} \quad (6)$$

Based on the obtained results from Equations (1), (3) & (4), the maximum value of the power inductance was selected as reference value for the power inductor prototype. The main goal is to ensure that the current ripple, ΔI_L is a small fraction of the full-load inductor DC component. In this study, the maximum value of inductance was found to be 2 mH.

4.3 Bi-directional converter control strategy

The converter control strategy shown in Figure-4 is such that if the DC bus voltage measured is higher than the reference voltage, then the current will flow from the bus to the battery to charge it (i.e. Buck converter). If the reference voltage is higher than the DC bus voltage, then the battery will discharge and current will flow from the battery to the bus (i.e. Boost converter).

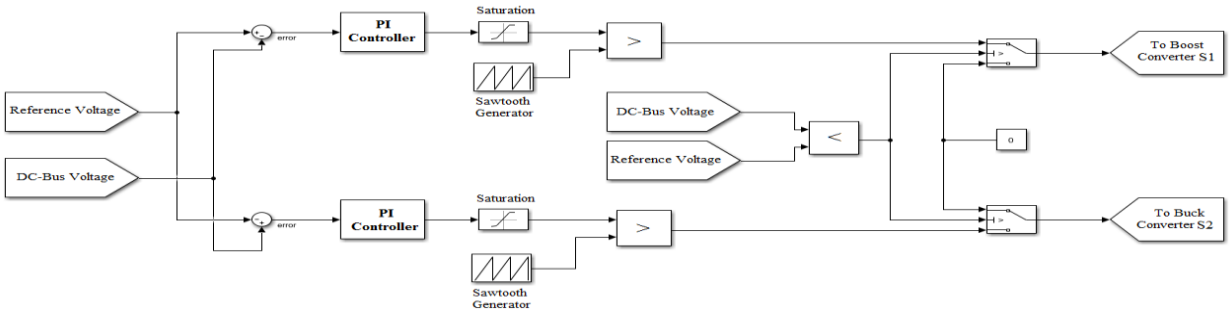

Figure-4. Bi-directional Buck-Boost converter control.

The PI controller and the saturation block are used to translate the error which resulted from the voltage comparison to a signal with a value between 0 and 1 (reference signal). Then this reference signal is compared with a sawtooth (carrier) signal to get the duty cycle used for switching the IGBT on and off.

4.4 Parasitic elements

The parasitic elements in a Buck-Boost converter are due to the losses associated with the inductor, the capacitor, the switches, and the diodes. Figure-5 shows that the parasitic elements have significant impact on the voltage conversion ratio and the stability of the converter. Unlike the ideal characteristic, in practice, V_0/V_d declines as the duty ratio approaches unity because of the very poor switch utilization at high values of duty ratio [13]. Because of these reasons, many designers won't use Boost or Buck factors higher than 6.

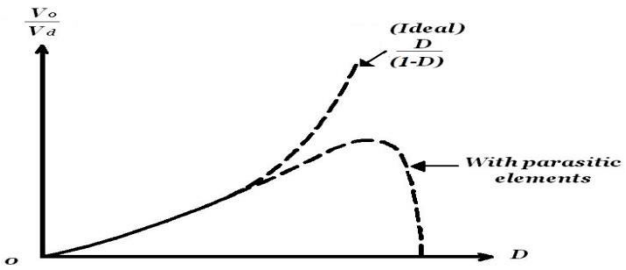

Figure-5. Effect of parasitic elements on the voltage conversion ratio of Buck-Boost converter.

5. LOAD POWER CALCULATION AND BATTERY SIZING

This section shows how to size your battery storage based on load power calculations. It's assumed that the irrigation water pump will be disconnected during the night and it only operates when the PV array is in service. The battery is sized based on domestic loads at night times when there's no sunlight, and hence there will be no power from PV array so the irrigation pump won't operate and won't be taken into account when sizing the battery pack.

5.1 Load power calculation

The following method calculates the domestic load power and energy required which is crucial for battery pack sizing.

Table-1 shows the battery and inverter voltages which will be needed for further calculations. The required energy/day for the loads specified is calculated in Table-2. The adjustment factor accounts for the conversion efficiency from DC to AC (inverter efficiency) which is 0.85, however, for DC loads this value is 1 as there is no inverter required. In this study, we have only AC loads. The load energy (A/h) and required wattage is calculated in Table-3.

Table-1. Battery and inverter voltages.

Symbol	Definition	Value
A1	Inverter efficiency	85 %
A2	Battery Bus voltage	128 V
A3	Inverter AC voltage (1-phase)	230 V
A4	Inverter AC voltage (3-phase)	400 V

Table-2. Load energy/day calculation.

Load type	Rated wattage (W)	Adjustment factor is 1.0 for DC, and (A1) for AC	Adjusted wattage (W) (A5/A6)	Hours/day used (h)	Energy/day (Wh) (A7xA8)
	Symbol				
	A5	A6	A7	A8	A9
(10) x 30w lights	300	0.85	353	12	4236
Refrigerator	500	0.85	589	5	2945
(3) x 45w fans	135	0.85	159	8	1272
Washing m/c	1500	0.85	1765	1	1765
TV	200	0.85	236	4	944
Other Appliances	1200	0.85	1412	6	8472

Table-3. Load energy and power requirement.

Symbol	Definition	Value
A10	Total energy demand per day (sum of A9)	19634 Wh
A11	Total amp-hour demand per day (A10/A2)	153.4 Ah
A12	Maximum AC power requirement (sum of A5)	3835 W
A13	Maximum DC power requirement (sum of A7)	4514 W

5.2 Battery sizing

Based on the calculations done in the previous section, the battery type and battery pack size are chosen.

In this study, the Valence U1-12XP (LiFeMgPO4) Lithium-ion battery [14] is chosen and taken as the reference battery for simulation because it offers intrinsic safety with twice the run-time and less than half the weight of similar sized lead-acid battery modules. Also, they can be cycled 100% and give about 2,500 cycles of service to 80% of initial capacity, and they are ideal when advanced energy systems are required for smart grid and distributed generation applications. Excellent float and cycle life with zero maintenance offers end users significant cost of ownership savings and complete peace of mind.

Table-4 shows the battery electrical specifications which are taken from the datasheet [14].

Table-4. Battery electrical specifications.

Parameter		Value
Rated Voltage		12.8 V
Rated Capacity (C/5, 23°C)		40 Ah
Standard Discharging at 25°C	Max. Continuous Load Current	80 A
	Peak Load Current (30 sec)	120 A
Standard Charging	Max. Charge Voltage	14.6 V
	Float Voltage	13.8 V
	Charge Time at 20 A	2.5 hrs
DC internal resistance (max)		15 mΩ

Where "C" rating is simply a battery's capacity (or Ah /amp hour rating)

Figure-6 shows the battery discharge characteristics [14], which is used to extract the remaining battery discharge parameters as indicated by their corresponding symbols in Table-5.

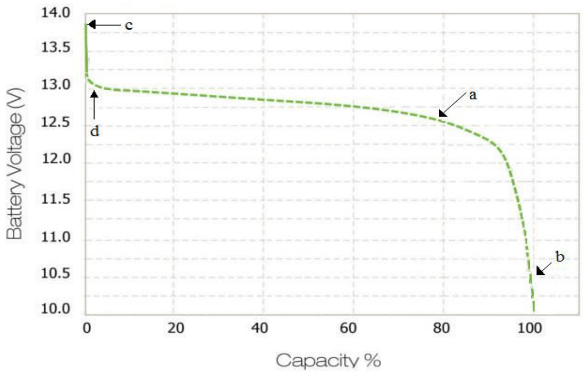

Figure-6. Battery discharging characteristics (C/2 rating (20A), 23°C).

Table-5. Extracted battery discharge parameters at (C/2).

Parameter	Denoted by	Value
Nominal Voltage (V)	a	12.6 V
Cut-off Voltage (V)	b	10.5 V
Fully Charged Voltage (V)	c	13.8 V
Capacity (Ah) at Nominal Voltage	a	30.14 Ah
Exponential zone [Voltage (V), Capacity (Ah)]	d	[13.1 V, 0.5 Ah]

- **Battery pack calculation**

The following method calculates the battery pack size based on load power and energy requirements as stated in the previous section, and also based on the specifications of the battery chosen. This is shown in Table-6.

Table-6. Battery pack calculation.

Symbol	Definition	Value
B1	Days of storage desired/required	5 days
B2	Allowable depth-of-discharge limit (decimal)	0.8
B3	Required battery capacity ((A11 x B1) / B2)	959 Ah
B4	Amp-Hour capacity of selected battery	40 Ah
B5	Number of batteries in parallel (B3 / B4)	24
B6	Number of batteries in series (A2 / battery voltage)	10
B7	Total Number of Batteries (B5xB6)	240
B8	Total battery amp-hour capacity (B5xB4)	960 Ah
B9	Total battery kilowatt-hour capacity (B8xA2)	122.9 KWh
B10	Average daily depth of discharge (1.0xA11/B8)	0.16

6. BATTERY SYSTEM CONTROL TOPOLOGY

The battery storage system has two modes of operation:

6.1 When the battery system is connected with the PV array to feed the motor pump

In this case, both the battery system and the PV array powers will be added together at the DC bus where the battery system will assist in achieving the pump hydraulic requirements freely without limitations and with no burden of having only one source of power (Standalone PV). The indirect field oriented control method is used here as shown in Figure-7.

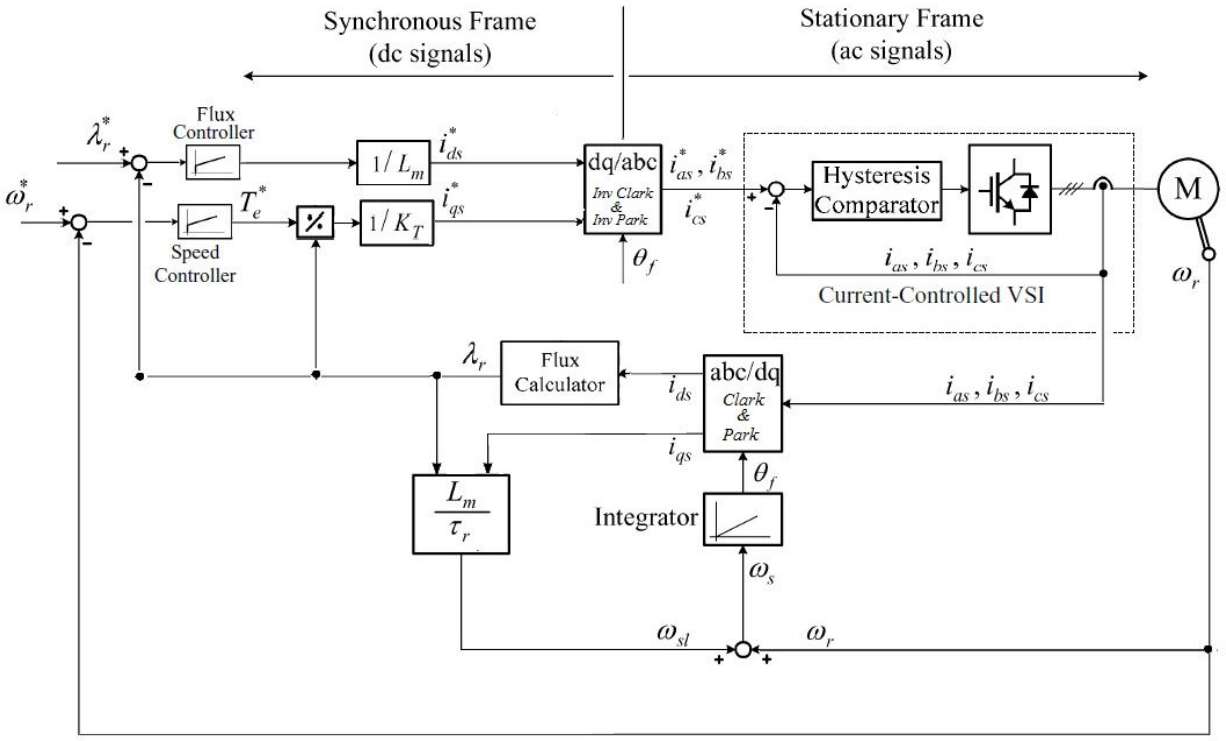

Figure-7. IFOC with a current regulated VSI.

When the PV power is higher than the load power, the PV system will feed the motor and the extra power will be used to charge the battery. When the PV power is less than the load power needed, the battery system will discharge and inject current into the DC bus to compensate for the remaining required power.

This, in turn, will help in reaping the full benefits of the Affinity laws [8] where the required motor power will change with changing the pumping head or the flow rate as can be seen in Equation (7).

$$\frac{Q_1}{Q_2} = \frac{N_1}{N_2}\ ,\ \frac{H_1}{H_2} = \left(\frac{N_1}{N_2}\right)^2\ ,\ \frac{P_1}{P_2} = \left(\frac{N_1}{N_2}\right)^3 \quad (7)$$

Furthermore, the bi-directional power transfer capability of the battery storage system and the Affinity laws will provide protection for the pump motor where the motor power will decrease when the pump motor speed decreases and vice versa.

This means that the load torque has a proportional relationship with the motor speed unlike when the motor was only fed from the fixed PV array power where they had an inversely proportional relationship. The relationship between the motor angular speed (ω), power (P) and load torque (T_L) is shown as extracted from the Affinity laws [8] in the following equations:

$$\frac{P_1}{P_2} = \frac{\omega_1 x T_{L1}}{\omega_2 x T_{L2}} = \left(\frac{\omega_1}{\omega_2}\right)^3 \quad (8)$$

$$\text{So:}\quad \frac{T_{L1}}{T_{L2}} = \left(\frac{\omega_1}{\omega_2}\right)^2 \quad (9)$$

As can be seen from the previous equations, the load torque is directly proportional to the square of the motor angular speed. This will keep the motor speed and load torque from exceeding their rated values and now we can use the Affinity laws fully without the limits or the restrictions that were set in the proposed method in [3] for the pump motor when it was fed from a fixed power standalone PV source.

6.2 When the battery system feeds the loads while the PV array is disconnected

At night when there is no sunlight, the PV modules will be disconnected from the system and the battery units will be the only source of power available.

In this study, we assumed that the water pump won't operate when the PV array is disconnected and so the battery will only feed the loads sized previously.

However, when there is no motor connected to the system, the field oriented control method won't be applicable in this situation. In this case, we need to switch to a control method that's able to generate the reference current necessary to control the inverter switches.

The control method used is the synchronous reference frame control [15]. This method monitors the load bus voltage. Consequentially, this voltage is transformed to its corresponding dq0 components using Clarke and Park transformations. The components of the load voltage are compared with the reference voltage dq0 components. This controller uses a three phase locked loop (PLL) to lock the grid frequency and phase angle. The load bus voltage should be kept sinusoidal with constant amplitude, and so the expected load bus voltage in the dq0 reference frame has only one value (V_{dref}) which is the peak value of the desired load voltage. This means that the d-axis of load reference voltage equals V_{dref}, while q-axis and 0-axis of the load reference voltage equal zero.

If a sag voltage is sensed, an error signal will be generated due to the difference between the measured and reference voltage values and the controller will be initiated in order to inject the missing voltage. This error signal drives a PI controller which controls the system depending on the actuating error signal. The output signal generated from the PI controller are dq0 voltages which are then forwarded to a voltage controller to convert them into dq0 currents. These currents are transformed back to three phase abc currents. These reference abc currents are then used with the currents generated from the active damping (AD) technique to control the inverter switches using the adaptive hysteresis current control method as explained in [9]. The proposed control method is shown in Figure-8.

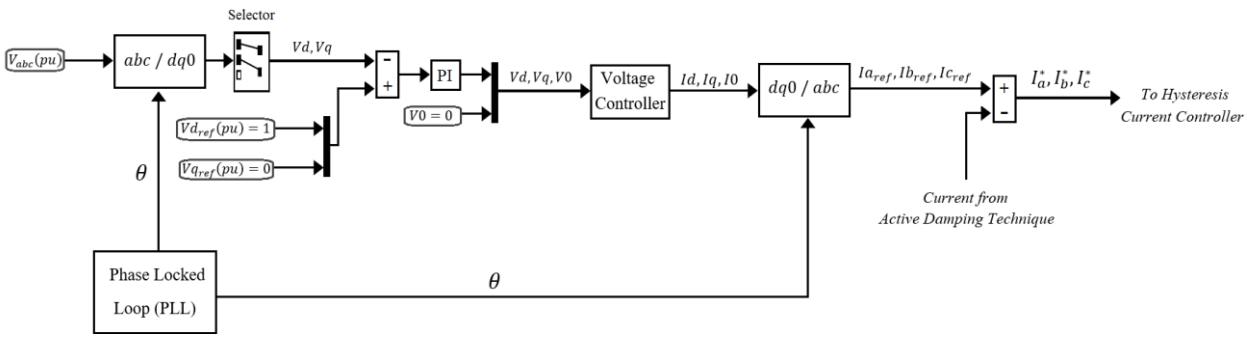

Figure-8. Synchronous reference frame control.

7. SIMULATION AND RESULTS

This section shows the simulation results using Matlab/Simulink software for the two cases mentioned in previous section. When the battery system is connected with the PV array to feed the motor pump at different hydraulic requirements and varying weather conditions, and when the battery system feeds the loads while the PV array is disconnected at two loading power conditions.

7.1 Simulation results for when the PV array and battery are feeding the motor

Figure-9 shows the Simulink model of the system when the pump motor is fed from both PV array and battery.

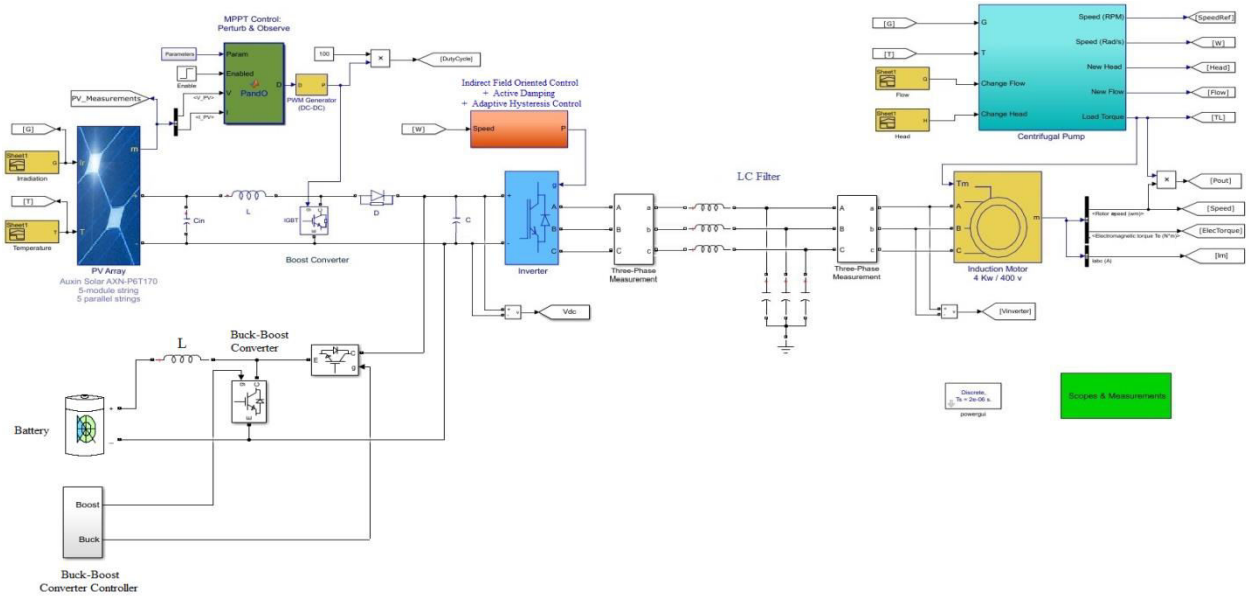

Figure-9. Matlab/Simulink model for the PV, battery and pump motor system.

Table-7 shows the motor speed and the required reference output power of the motor (Pout_ref) to realize the varying hydraulic requirements (flow rate (Q) and pumping head (H)) over the simulation time. It also shows that the weather conditions (irradiance (G) and temperature (T)) will be varied during the simulation.

Table-7. The G, T, Q, H, Pout_ref and speed variation over the simulation time.

Time (secs)	**G** (W/m²)	**T** (ºC)	**Q** (m³/h)	**H** (m)	**Pout_ref** (kw)	**Motor Speed** (RPM)
0-0.2	1000	25	110	7.6	3.63	1425
0.2-0.4	1000	30	92.6	5.39	2.167	1200
0.4-0.6	900	30	100.35	6.325	2.756	1300
0.6-0.8	900	35	84.9	4.528	1.67	1100
0.8-1.0	1000	35	69.47	3.03	0.915	900
1.0-1.2	1000	25	104.2	6.82	3.08	1350
1.2-1.3	500	25	104.2	6.82	3.08	1350
1.3-1.5	500	25	110	7.6	3.63	1425
1.5-2.0	1000	25	38.59	0.935	0.156	500

Figure-10 shows the irradiance and temperature variations throughout the simulation time where these would affect the PV output power. It also shows that the hydraulic requirements (flow rate and head) will be varied.

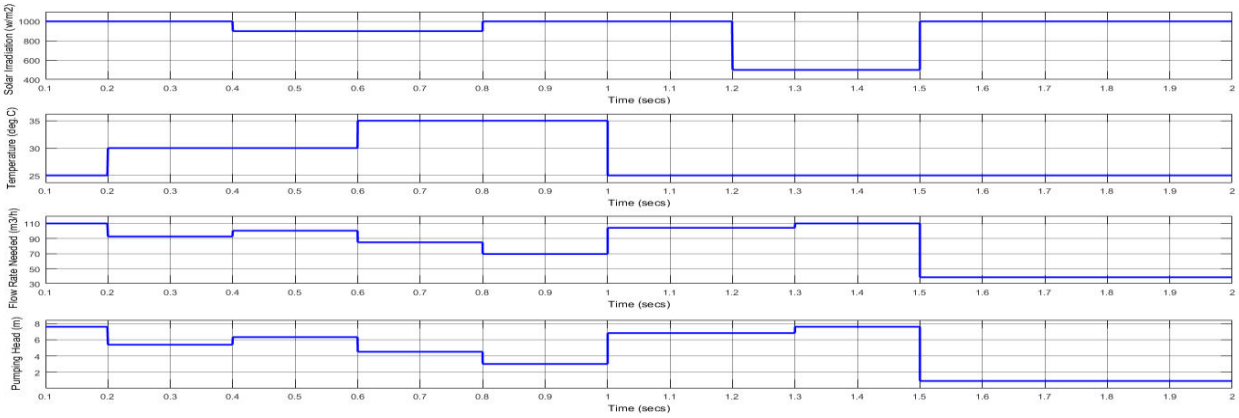

Figure-10. G, T, Q and H variations.

Due to the hydraulic requirements variations seen in Figure-10, the required motor output power (Pout_ref) will vary. Figure-11 shows the required DC bus power which is the summation of the PV power (Ppv) and the battery power (Pbatt), with Ppv fluctuating due to the weather conditions variations. Furthermore, it shows that the measured motor output power (Pout) follows Pout_ref with great accuracy which shows the merits of the battery connection.

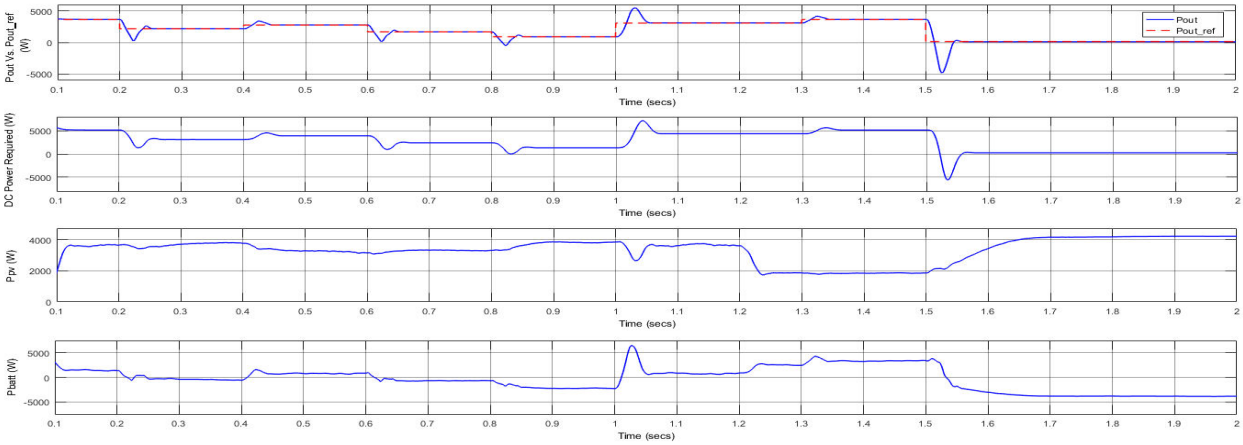

Figure-11. Ppv, Pbatt, DC power required and Pout.

Figure-12 shows the motor speed (N) and its corresponding electromagnetic torque (Te) will vary throughout the simulation time to realize the required hydraulic performance. It also shows the motor terminal voltage (V) and the motor current (I) during that period.

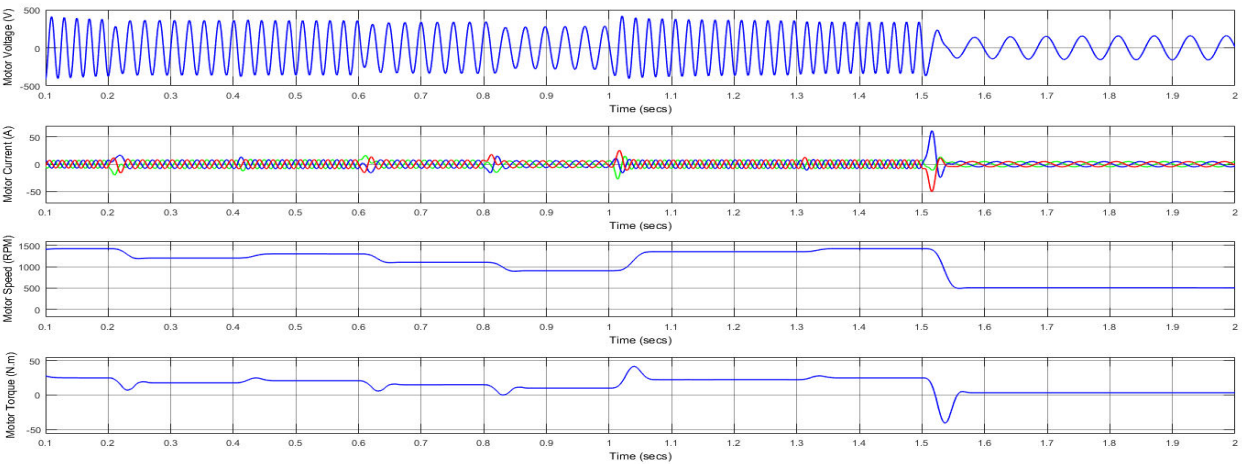

Figure-12. V, I, N and Te variations.

As can be seen in Figure-13, the motor actual speed (N) follows the required reference speed with fast response and good accuracy.

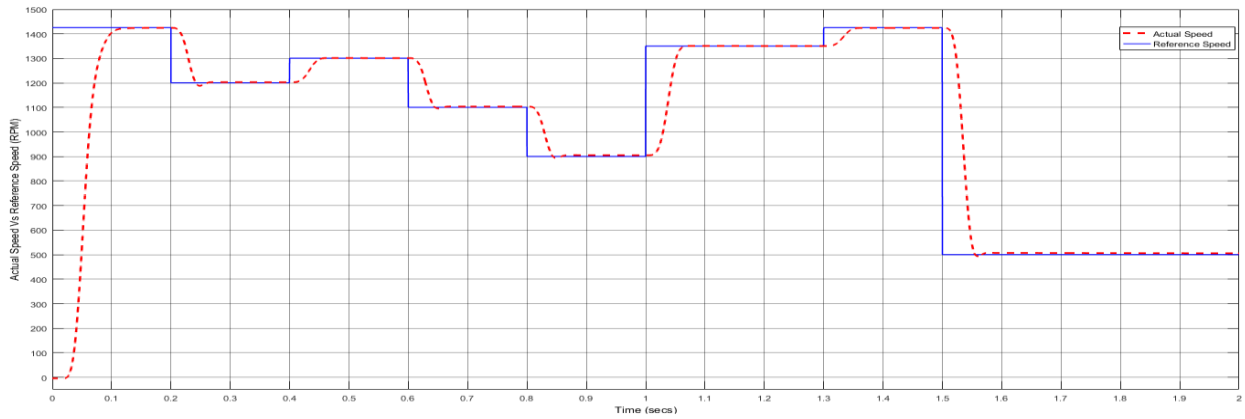

Figure-13. Performance of motor actual speed vs. required reference speed.

Figure-14 shows the battery voltage (Vbatt), current (Ibatt) and state of charge (SOC) throughout the simulation time. It can be seen that when the PV power is less than what is required by the load, the battery will discharge to compensate for the needed power. On the other hand, when PV power is more than what is required, the battery will charge.

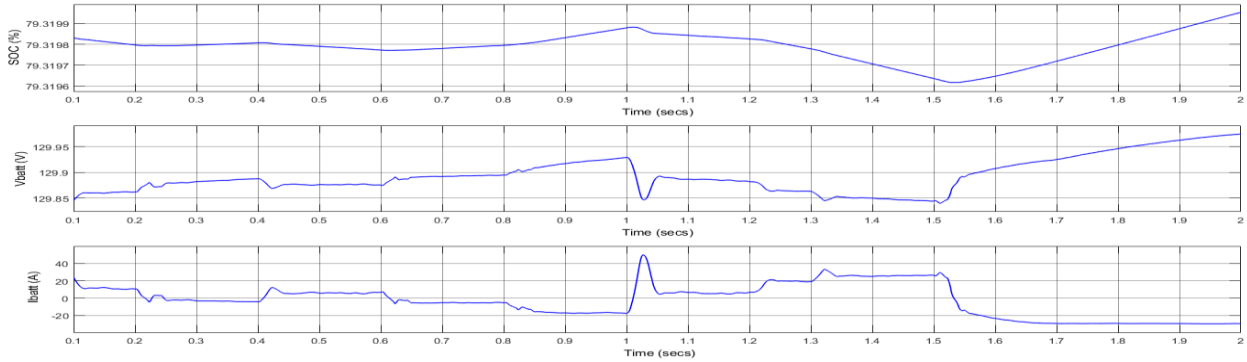

Figure-14. Vbatt, Ibatt and SOC.

7.2 Simulation results when the battery only is feeding the load

Figure-15 shows the Simulink model of the system when only the battery is feeding the domestic loads while PV array is disconnected from the system, and also, the water pump is not in operation. In this case, the inverter will adopt the synchronous reference frame control method. Furthermore, there are two loading situations where the first is the maximum loading condition as previously calculated, and the second loading condition is at nearly half the maximum load.

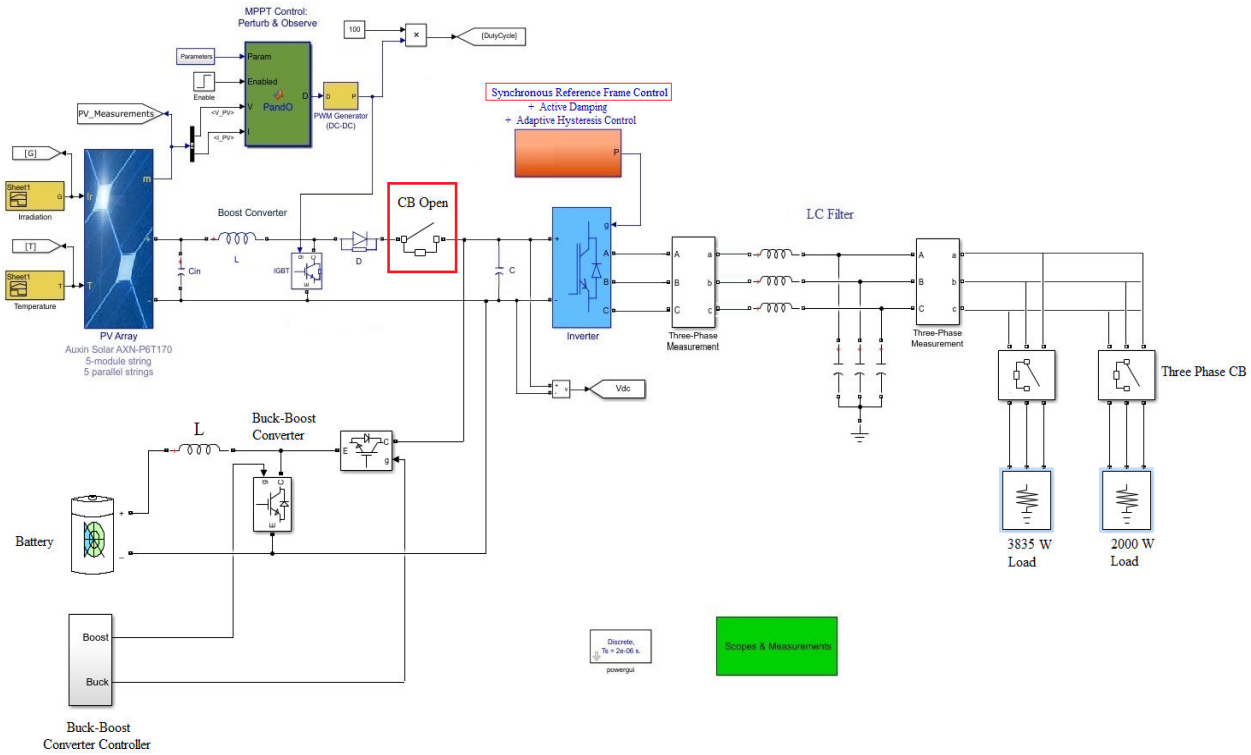

Figure-15. Matlab/Simulink model for the battery feeding domestic loads.

The simulation will start with the load is at its maximum of 3835 W and then the load will drop to 2000 W when the simulation time is at 0.6 as can be seen inFigure-16.

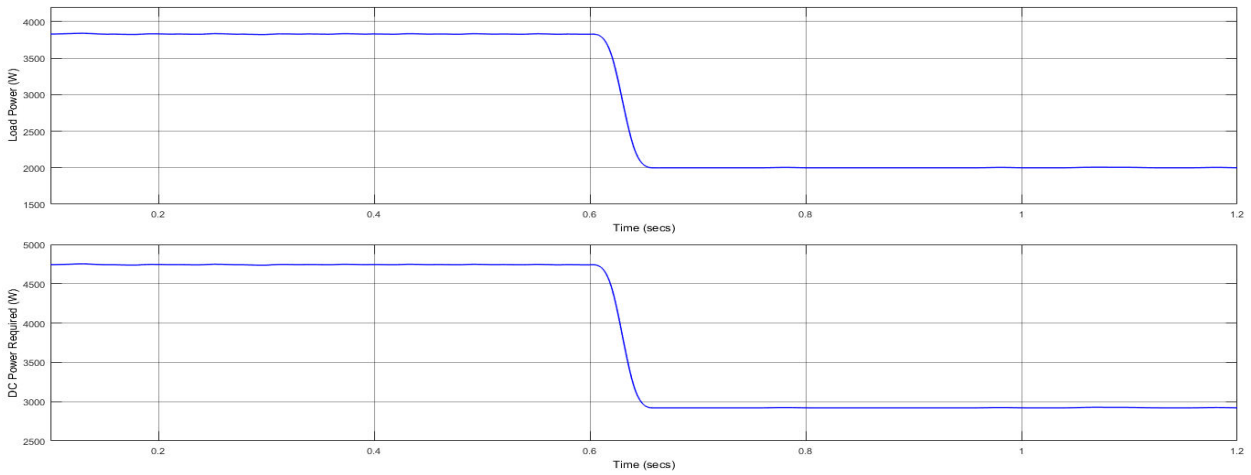

Figure-16. Load power and DC power required.

Figure-17 shows the load voltage and current. It is noticed that the voltage is kept constant even when the loading is cut in half during simulation.

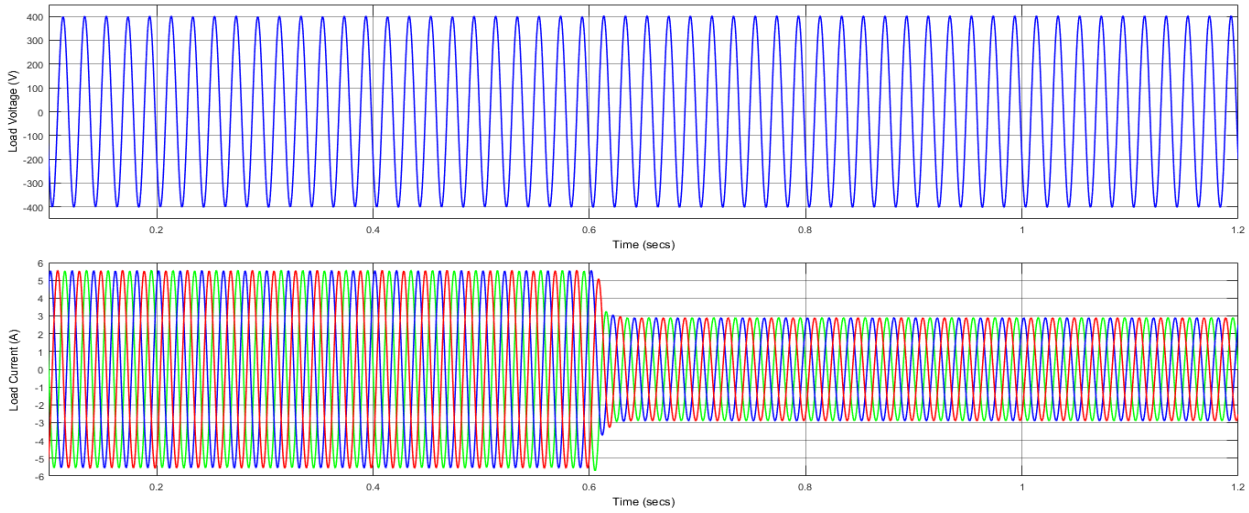

Figure-17. Load voltage and current.

Figure-18 shows the battery voltage (Vbatt), current (Ibatt) and state of charge (SOC). As can be seen, when the loading conditions decrease, the current discharged from the battery is decreased and the slope of SOC is decreased.

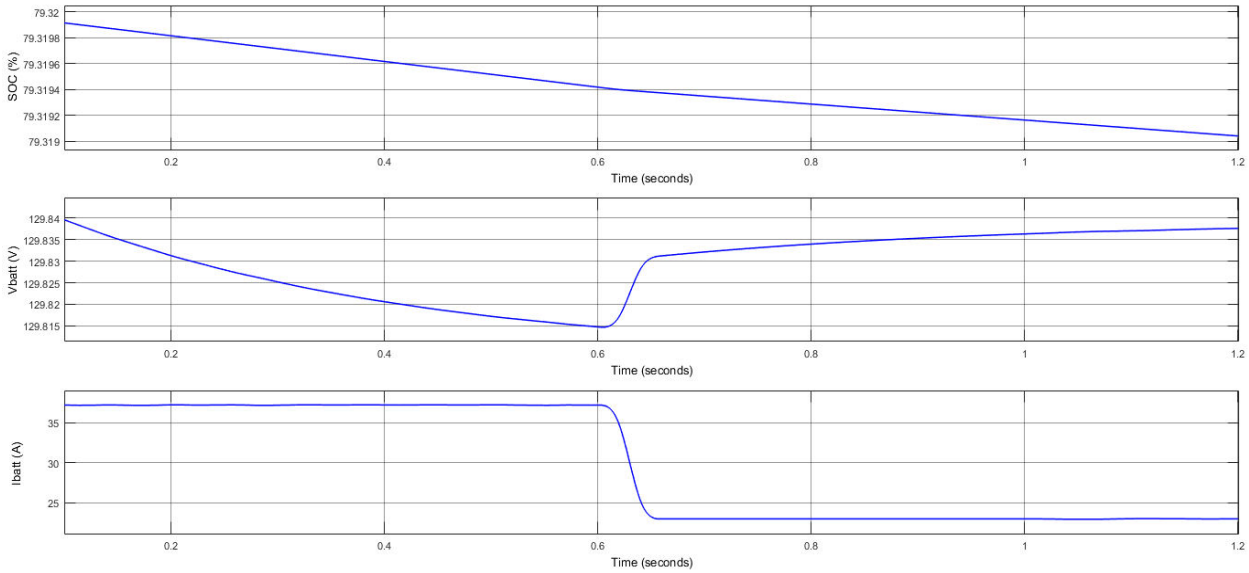

Figure-18. Vbatt, Ibatt and SOC when only the battery is feeding the load.

8. CONCLUSIONS

A battery energy storage system has been modeled and designed to compensate for the intermittency related to PV power in order to achieve the load requirements. Moreover, it examines the use and control of the bi-directional Buck-Boost converter for energy management between the battery and system. Domestic loads power calculation and battery sizing are also presented. Two cases were studied: when the battery system is connected with the PV array to feed the pump motor to achieve the required hydraulic performance, and when the battery system feeds the loads while the PV array is disconnected at the night. Finally, the synchronous reference frame control method was presented for inverter control when the battery is the only source of power in the system.

REFERENCES

[1] Sawin Janet L., Sverrisson Freyr, Seyboth Kristin, Adib Rana, Murdock Hannah E., Lins Christine, Edwards Isobel, Hullin Martin, Nguyen Linh H., Prillianto Satrio S., Satzinger Katharina, Appavou Fabiani, Brown Adam, Chernyakhovskiy Ilya, Logan Jeffrey, Milligan Michael, Zinaman Owen, Epp Baerbel, Huber Lon, Lyons Lorcan, Nowak Thomas, Otte Pia, Skeen Jonathan, Sovacool Benjamin, Witkamp Bert, Musolino Evan, Brown Adam,

Williamson Laura E., Ashworth Lewis & Mastny Lisa. 2017. Renewables 2017 Global Status Report (INIS-FR-17-0569).

[2] Chandel S. S., M. Nagaraju Naik and Rahul Chandel. 2015. Review of Solar Photovoltaic Water Pumping System Technology for Irrigation and Community Drinking Water Supplies. Renewable and Sustainable Energy Reviews. 49: 1084-1099.

[3] Moubarak A., G. El-Saady and El-Noby A. Ibrahim. 2017. Variable Speed Photovoltaic Water Pumping Using Affinity Laws. Journal of Power and Energy Engineering. 5: 50-71.

[4] M. A. G. de Brito, L. Galotto, L. P. Sampaio, G. de Azevedo e Melo, and C. A. Canesin. 2013. Evaluation of the Main MPPT Techniques for Photovoltaic Applications. IEEE Transactions on Industrial Electronics. 60(3): 1156-1167.

[5] M. Forouzesh, Y. P. Siwakoti, S. A. Gorji, F. Blaabjerg, and B. Lehman. 2017. Step-Up DC–DC Converters: A Comprehensive Review of Voltage-Boosting Techniques, Topologies, and Applications. IEEE Transactions on Power Electronics. 32(12): 9143-9178.

[6] Caracas J.V.M., G. de Carvalho Farias, L.F.M. Teixeira and L.A. de Souza Ribeiro. 2014. Implementation of a High Efficiency, High-Lifetime, and Low-Cost Converter for an Autonomous Photovoltaic Water Pumping System. IEEE Transactions on Industry Applications. 50: 631-641.

[7] B. Wu. 2006. High-Power Converters and AC Drives. 1st Edition, Wiley-IEEE Press, New York, USA.

[8] J. P. M. Igor, J. Karassik, P. Cooper, and C. C. Heald. 2008. Pump Handbook. 4th Edition, McGraw-Hill, New York, USA.

[9] Moubarak A., G. El-Saady and El-Noby A. Ibrahim. 2018. Power Quality Improvement of Photovoltaic Water Pumping System Using LC Filter. ARPN Journal of Engineering and Applied Sciences. 13(4):1311-1326.

[10] Tremblay O. and L. A. Dessaint. 2009. Experimental Validation of a Battery Dynamic Model for EV Applications. World Electric Vehicle Journal. 3(1): 1-10.

[11] Shepherd C. M. 1965. Design of Primary and Secondary Cells II. An Equation Describing Battery Discharge. Journal of the Electrochemical Society. 112(7): 657-664.

[12] Perdigão M. S., J. P. F. Trovão, J. M. Alonso and E. S. Saraiva.2015. Large-Signal Characterization of Power Inductors in EV Bidirectional DC–DC Converters Focused on Core Size Optimization. IEEE Transactions on Industrial Electronics. 62(5): 3042-3051.

[13] N. Mohan, T. M. Undeland and W. P. Robbins. 2003. Power Electronics: Converters, Applications, and Design. 3rd Edition, Wiley, New York.

[14] Valence. 2012, Aug. U1-12XP. https://www.celltech.se/fileadmin/user_upload/Celltech/Products/Litium_laddningsbara/Valence_Modules/XP_Module_Datasheet.pdf

[15] Khaburi D. A. and A. Nazempour. 2012. Design and Simulation of a PWM Rectifier connected to a PM Generator of Micro Turbine Unit. Scientia Iranica. 19(3): 820-828.